DOI: 10.61782/fa.2025.0274

FORUM ACUSTICUM
EURONOISE 2025

DESIGN AND VALIDATION OF AN ACOUSTO-OPTIC TUNABLE FILTER FOR SPECTRO-POLARIMETRY ANALYSIS

Samuel Dupont[1*] **Jurgen Vanhamel**[2,3] **Jean-Claude Kastelik** [1]
[1] Université Polytechnique Hauts-de-France (UPHF), IEMN – Campus Mont Houy – Cedex 9, 59313 Valenciennes, France
[2] TU Delft - Faculty of Aerospace Engineering, Kluyverweg 1, 2629 HS Delft, The Netherlands
[3] Electronic Circuits and Systems, KU Leuven, Kleinhoefstraat 4, 2440 Geel, Belgium

ABSTRACT

Acousto-Optic Tunable Filters (AOTF) are versatile devices with a range of applications in modern optics. Their technology has reached a mature industrialability. They are particularly valuable in fields requiring precise wavelength selection and fast switching capabilities, making them essential tools in various applications. The generalisation of their use has led to new applications still requiring specific developments.
We present the design and validation of an AOTF for spectro-polarimetry analysis which provides a constant spectral resolution over a wide spectral band. The variation of the spectral resolution is made possible by the manufacture of a transducer divided into multiple electrodes allowing to play on the interaction length easily by activating and deactivating the electrodes. In addition, the power distribution supplying the electrodes can be modulated, which offers the possibility of finely controlling the spectral template.
The device developed has an acoustic cut of 5°, operating from 450 to 800 nm. We opted for a transducer equipped with 5 electrodes. This strategy makes it possible, depending on the power supply conditions, to modulate the selectivity of the filter by a factor of 4 for a given wavelength and to maintain a constant selectivity of the order of 10 nm over the entire operating range.

Keywords: *AOTF, multi-electrodes, spectro-polarimetry.*

1. INTRODUCTION

Optical filters are essential components in various applications, including telecommunications, sensing, imaging, and spectroscopy [1]. Among these technologies, AOTF have emerged as an useful tool, allowing for precise control over the spectral characteristics of light [2]. Those devices have attracted a great interest, for example, the use of AOTF in imaging applications is under constant development [3-7].
Like all acousto-optic components, the design of the filters is subject to compromise depending on the intended use. For example, some applications require a large angular aperture, others require a large spectral band, while others require large rejection. The optical spectral filter function of an AOTF is a cardinal sine: it has a main lobe and adjacent secondary lobes. The side lobes reduce the performance of the filters by creating diaphony. This is a secondary aspect when filtering monochromatic signals, but it becomes an issue when we are in the presence of a wide spectral band signal. In this case, when tuning the filter for a given wavelength, it is possible to achieve a diffraction efficiency for a neighboring wavelength of up to 10%. In imaging, these secondary lobes are unwanted because they make the image blurry [6]. It is then necessary to reduce the adjacent lobes by implementing an apodization technique. Also, emerging applications drive advancements developments in spectro-polarimetry optical technologies. Spectro-polarimetry combines spectral and polarization information and becomes essential for various scientific fields, including materials science, biology, and remote sensing. The ability to tune the

[*] ***Corresponding author***: Samuel.dupont@uphf.fr

filter dynamically, as offered by acousto-optic technologies, enhances the versatility and efficiency of spectro-polarimetric measurements, allowing for real-time analysis of complex samples.
This study centers on the development of an apodised AOTF specifically tailored for spectro-polarimetry applications. We present the development of the AOTF, detailing the operational principle, the design parameters and the experimental validation.

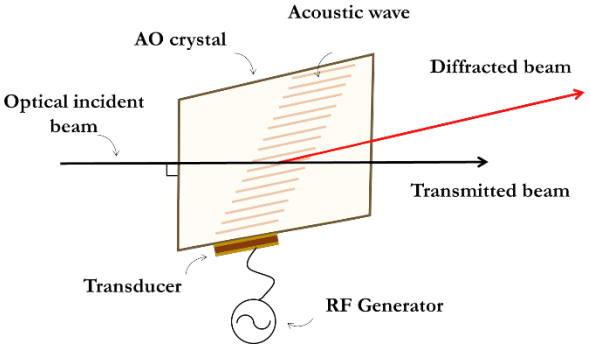

Figure 1. AOTF cell schematic view.

2. AOTF DESIGN

AOTFs are compact and efficient devices able to filter specific optical wavelengths with precision by the application of an appropriate Radio-Frequency (RF) signal that is tuned to satisfy the Bragg matching conditions for diffraction. In order to operate the AOTF, a piezoelectric transducer is mounted onto the side of a photoelastic crystal, such as in our case Tellurium Dioxide (TeO_2), figure 1. This transducer operates by converting RF signals into corresponding sound waves. By applying the appropriate frequency and power level to the transducer, the Bragg matching condition can be successfully satisfied: two first-order diffracted light beams are then separated at the output of the crystal for light with a precisely defined optical wavelength.

2.1 Bragg diffraction

Under Bragg phase matching conditions, the incident and diffracted optical wave vectors (k_i, k_d) and the acoustic wavevector (K) satisfy the exact momentum conservation:

$$\overrightarrow{k_d} = \vec{K} + \overrightarrow{k_i} \quad (1)$$

When the conditions exit the exact conditions (figure 2), a phase mismatch appears, it corresponds to a momentum offset Δk_d:

$$\overrightarrow{k_d} = \vec{K} + \overrightarrow{k_i} + \overrightarrow{\Delta k_d} \quad (2)$$

The study of these conditions allows to obtain information on the angles (incident and diffracted), the wavelength and the acoustic frequency of the interaction, since these parameters are related. With $\Delta\Phi = \Delta k_d . W_{eff}$ the phase mismatch and W_{eff} the effective interaction length that is given by:

$$W_{eff} = \frac{W\cos(\psi)}{\cos(\psi - \theta_i + \theta_a)} \quad (3)$$

Phase mismatch can come from several parameters: a variation in the wavelength $\Delta\lambda$ (spectral bandwidth); a variation in frequency Δf (frequency bandwidth); a variation of the incident angle (angular acceptance): $\Delta\theta$.

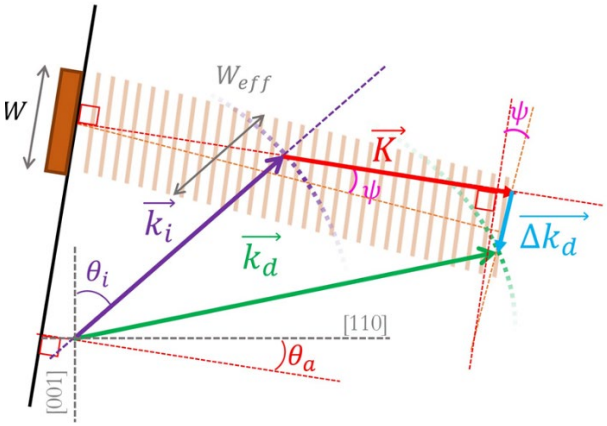

Figure 2. Wave vector diagram.

2.2 AOTF diffraction efficiency

The diffraction efficiency η of an acousto-optic component is expressed by:

$$\eta = \frac{P}{P_0}\frac{\sin^2\left(\frac{\pi}{2}\sqrt{\frac{P}{P_0}+\left(\frac{\Delta\Phi}{\pi}\right)^2}\right)}{\frac{P}{P_0}+\left(\frac{\Delta\Phi}{\pi}\right)^2} \quad (4)$$

The efficiency depends on the sound power P and the phase mismatch $\Delta\Phi$. As we are talking about a filter here, we are interested in the impact of the parameters on the filter optical spectral characteristics.
The analysis of the evolution of the diffraction efficiency as a function of wavelength, angle of incidence or acoustic frequency makes it possible to determine, respectively: an optical (or spectral), angular or acoustic bandwidth (Figure 3). The secondary lobes that characterize the rise in diffraction efficiency on either side of the main lobe can be determined in each of these cases.

An example of the typical diffraction efficiency evolution is shown in Fig. 3.

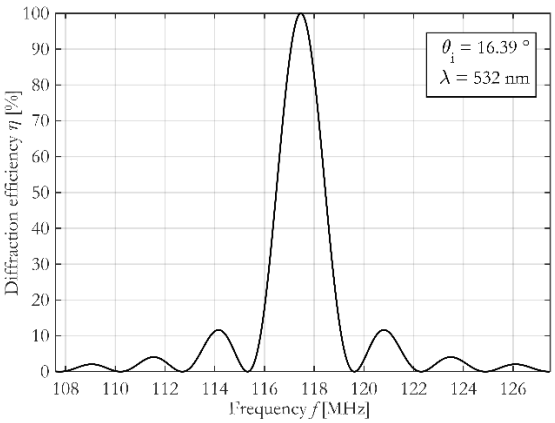

Figure 3. AOTF diffraction efficiency as a function of acoustic frequency.

The diffraction efficiency curves have a recognizable profile: a main lobe and side lobes for representation as a function of acoustic frequency or optical wavelength.
By exploiting the vector relation, it is possible to determine the expression of the acoustic frequency. If the interaction is from ordinary to extraordinary mode, it is expressed by [3]:

$$f_S = \frac{V}{\lambda}\sigma\left(n_i(\theta_i)\sin(\theta_i - \theta_a) - \sqrt{{n_d}^2(\theta_d) - {n_i}^2(\theta_i)\cos^2(\theta_i - \theta_a)}\right) \quad (5)$$

The frequency equation is a function of the parameters of the component and the interaction configuration: angle of incidence θ_i, acoustic cut θ_a, optical wavelength λ, acoustic velocity V, refractive indices ${n_i}^2$ and ${n_d}^2$.

It can be seen in Figure 4, which shows the different acoustic frequencies for extraordinary to ordinary (e-o) and ordinary to extraordinary (o-e) cases as a function of the angle of incidence, that the interaction frequency has some interesting particularities:
-It increases non-linearly if the wavelength decreases; -the two curves intercept.
-There is an incident angle for each frequency curve for which the variation around that angle does not cause a large frequency variation. This angle is the angle necessary to be in a particular case: the case of parallel tangents.
-The curves representing the two modes of interaction intersect at a single point, this is the point of the double interaction, where 100% of the polarizations are diffracted.
Also, it should be noted that the coordinate of the double interaction increases if the acoustic cut increases.

2.3 Apodisation of AOTF transfer function

Figure 3 clearly demonstrates that secondary lobes can be a limiting factor when monochromaticity of the filter is required. This is particularly relevant in the field of spectral imaging [6]. An interesting technic consists in the fabrication of a phased array transducer to control the acousto-optic transfer function [8, 9].
The principle of apodization in AOTFs with arrayed transducers involves the shaping of the acoustic wave's amplitude distribution to influence the diffraction pattern of light. By feeding the array transducer with a Gaussian power distribution, the acoustic wave's intensity generated tapers off gradually towards the edges, reducing abrupt transitions that cause side lobes in the optical output. Indeed, the acoustic wave generates the modulation of the refractive index of the medium, which acts as a diffraction grating for the incident light. The Gaussian power distribution across the transducers ensures that the acoustic wave's amplitude decreases symmetrically from the centre to the edges, so does the diffraction grating strength, minimizing the side lobes in the resulting optical transmission function.
There is of course a tradeoff between system complexity and the achievable filtering characteristics: using a large number of elements allows for a finely tuned filter transfer function with significant side lobe reduction, but it requires a more complex radiofrequency generator capable of producing as many radiofrequency tones as there are elements. We have established that even three elements can enhance the filtering characteristics of an AOTF [10]. To further improve these characteristics while keeping system complexity at an acceptable level, we have developed a device with five transducer elements.
The 5 electrodes can be activated independently, which allows the interaction length W_{eff} to be varied and therefore the optical spectral resolution $\Delta\lambda$ to be varied. This also allows for an apodization functionality.
To design the filter, it is useful to understand how the spectral and frequency bandwidths vary with different parameters. These variations depend on the acoustic cut, which is the first element we examine.

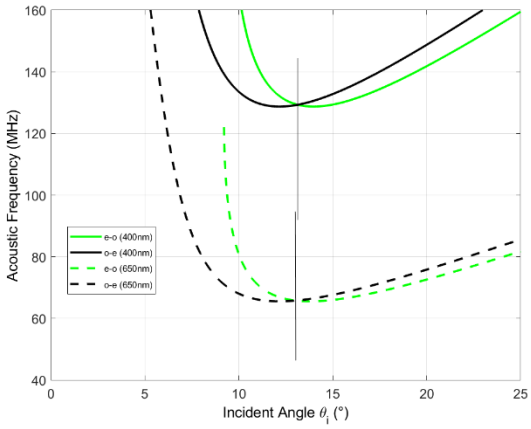

Figure 4. Evolution of the acoustic frequency at synchronism as a function of incident angle (acoustic cut considered for illustration: 6°).

3. DESIGN OF THE AOTF

Here, we present the design considerations for an AOTF operating in the visible light range, hence targeting an operational bandwidth from 400 nm to 900 nm at the design stage. Due to its high efficiency, paratellurite is chosen as the acousto-optic material.

3.1 Analysis of AOTF parameters

Figure 5 shows the variation of acoustic frequency across the reference spectral band for several acoustic cuts ranging from 3° to 9°. It can be observed that the frequency decreases as the wavelength increases, and this effect becomes more pronounced with larger acoustic cuts. High acoustic cuts necessitate higher radiofrequency operation, while low acoustic cuts are known to be more susceptible to unwanted gyrotropy effects [11].

Spectral resolution is a key criterion when selecting the acoustic cut for an AOTF. Figure 6 illustrates how spectral resolution varies with wavelength for several acoustic cut angles, assuming an effective acoustic column width of 7 mm. As can be seen, higher acoustic cuts result in lower spectral resolution. Moreover, a strong variation in spectral resolution is observed for small acoustic cuts; therefore, cuts of 4° or less were excluded, as they correspond to filters with optical resolution profiles that can reach up to 35 nm. However, a filter that would be too selective would result in low diffracted power. Hence, the higher cuts are neither favorable.

We have selected a 5° acoustic cut, which is sufficient to prevent gyrotropy effects while keeping the radiofrequency range confined within a single octave for a practical operation range from 450 nm to 800 nm and offer acceptable spectral resolution.

Then the choice of the number and the width of the electrodes should be considered. We first consider a single electrode of width comprised between 2 to 11 mm. Figure 7 illustrates the variation of spectral resolution with wavelength for various transducer lengths W. It can be observed that this electrode width enable a spectral resolution of approximately 10 nm across the entire operating band, with operation ranging from a 2 mm electrode at 450 nm to an 11 mm electrode at 800 nm. Since the number of electrodes is limited to five to enable spectral tunability while keeping system complexity at an acceptable level, we selected a central electrode larger than the others: 3 mm compared to 2 mm for the rest. This configuration allows, by activating adjacent electrodes, the formation of total transducer lengths of 2, 3, 4, 5, 7, 9, and 11 mm. By selecting, for example, only the 3 to 11 mm configurations, the spectral resolution varies by just a few nanometers across the entire optical band, ranging from approximately 8 to 11 nm, resulting in a variation factor of only 1.4 between the highest and lowest wavelengths.

Finally, considering the double operation point, an incident angle of 10.83° is required. A picture of the device is shown figure 8 and the parameters are summarized in table 1.

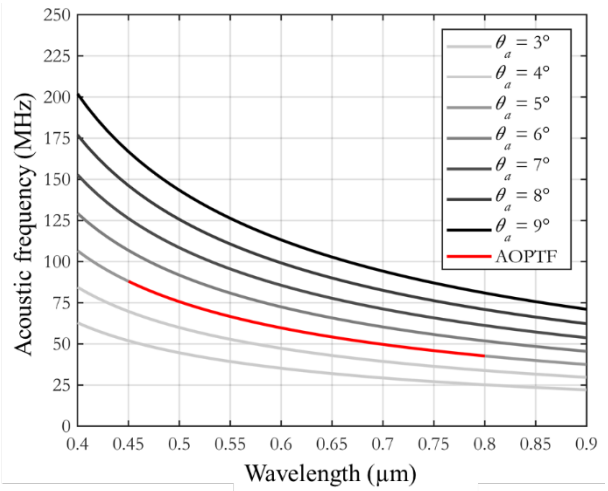

Figure 5. Evolution of acoustic Bragg frequency as a function of wavelength for acoustic cuts from 3° to 9°.

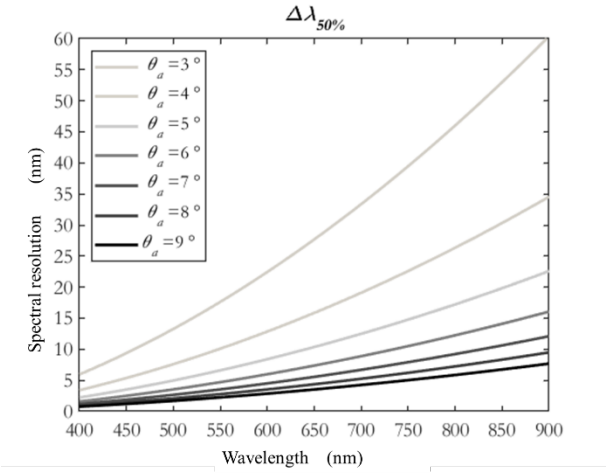

Figure 6. Evolution of AOTF spectral resolution as a function of wavelength for different acoustic cuts.

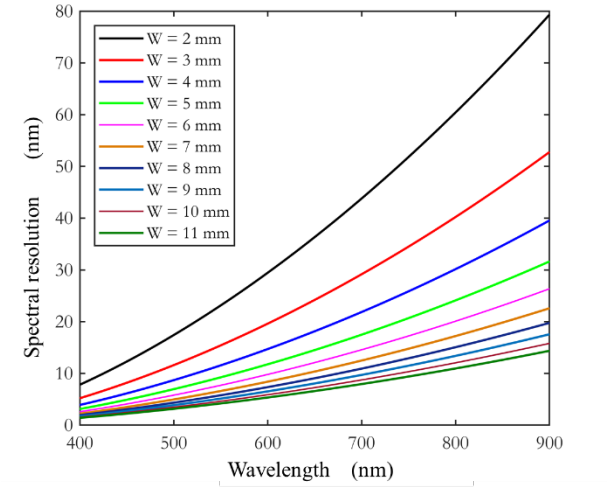

Figure 7. Evolution of spectral resolution for various transducer length.

Table 1. AOTF parameters.

Variable	Value	Unit
Acoustic cut θ_a	5	Degrees
Incident angle θ_i	10.83	Degrees
Transducer length	2 to 11	mm
Transducer number	5	

3.2 AOTF experimental validation

An experimental characterization of the AOTF was performed using the 514 nm line from an argon-ion laser. The same RF signal is coupled to all electrodes. Note that a phase shifter is introduced on the central electrode to compensate for its different behavior, due to its wider width compared to the other transducers. The AOTF's transfer function was estimated by scanning the RF signal across the Bragg frequency, a method known to approximate the optical transfer function shape. Figure 9 shows the relative efficiency of the AOTF for electrode widths ranging from 3 to 11 mm. As expected, a longer grating results in a reduced spectral bandwidth.
The apodization capability was then tested using a 5-channel RF generator developed in house, and an illustration of the apodized filter response is shown in Figure 10.

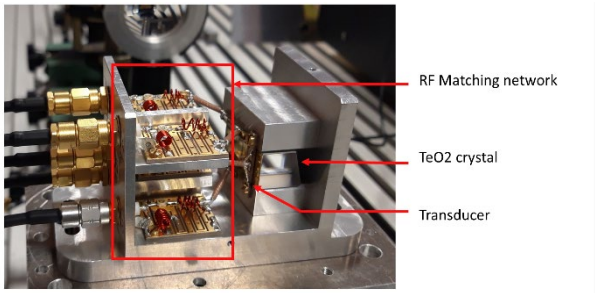

Figure 8. View of the AOTF.

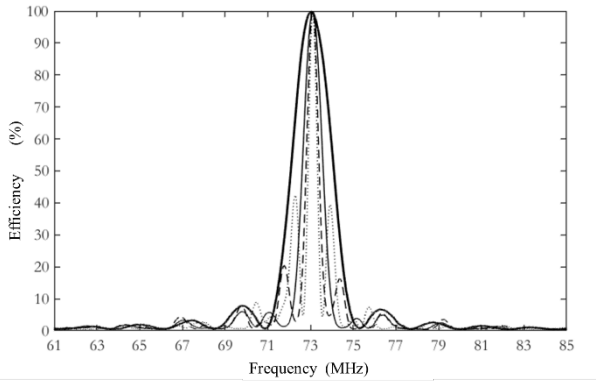

Figure 9. AOTF relative efficiency measured at 514 nm as a function of rf frequency for transducer width activated from 3 to 11 mm.

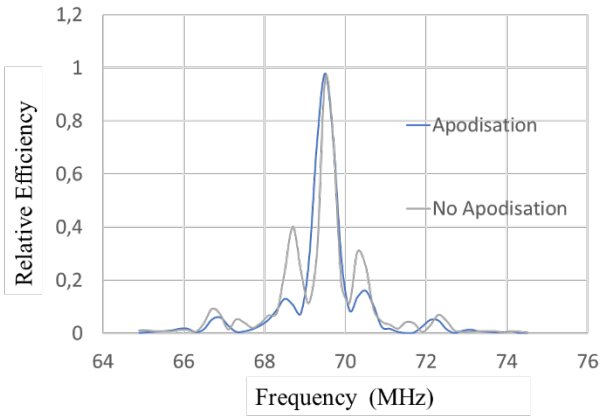

Figure 10. Test of apodisation capability at 532 nm.

During the apodization test, the power distribution across the five electrodes follows a Gaussian-like pattern, while the relative phase between the electrodes is adjusted to compensate for differences between the channels.

4. CONCLUSIONS

In this paper, we have outlined the key steps involved in the design and validation of an acousto-optic tunable filter capable of functioning as a spectropolarimeter. Simulation results were analysed to assess efficiency variations as a function of several parameters. Based on this analysis, an AOTF was designed and implemented to operate within the visible spectrum, from 450 nm to 800 nm. The device features five electrodes, enabling control of spectral resolution as a function of wavelength to achieve a nearly constant resolution across the entire operating range. Characterization and validation confirmed that the component met performance expectations, demonstrating that spectral resolution can be easily adjusted by activating multiple electrodes. With a resolution of approximately 10 nm, the system can distinguish up to 35 discrete spectral bands.

5. ACKNOWLEDGMENTS

The authors would like to thank F. Rivart for the fabrication of R.F. generator and the Delft University of Technology (TU Delft) and the Université Polytechnique Hauts-de-France (UPHF), to accommodate this collaboration and experimental work.

6. REFERENCES

[1] CHANG, I. C. Acousto-optic devices and applications. *Handbook of optics*, 1995, vol. 2, p. 12.1-12.54.

[2] GUPTA, Neelam. Acousto-optic tunable filters. *optics and Photonics News*, 1997, vol. 8, no 11, p. 23-27.

[3] V. B. Voloshinov, V. Y. Molchanov, and J. C. Mosquera, "Spectral and polarization analysis of optical images by means of acousto-optics," *Optics & Laser Technology*, vol. 28, no. 2, pp. 119–127, 1996.

[4] E. Dekemper, J. Vanhamel, B. Van Opstal, and D. Fussen, "The AOTF-based NO2 camera," *Atmospheric Measurement Techniques*, vol. 9, no. 12, pp. 6025-6034, 2016.

[5] Dan R. Lobb "Wide-angle optical systems with moderate spectral resolution, for monitoring the oceans from low Earth orbit", Proc. SPIE 5962, Optical Design and Engineering II, 59621K (14 October 2005)

[6] GUPTA, Neelam et SUHRE, Dennis R. Effects of sidelobes on acousto-optic tunable filter imaging. *Optical Engineering*, 2017, vol. 56, no 7, p. 073106-073106.

[7] POLIAKOV, M. P., BATSHEV, V. I., MACHIKHIN, A. S., et al. Unified optical scheme of an acousto-optical imaging spectrometer for the visible spectrum. *Journal of Optical Technology*, 2024, vol. 90, no 11, p. 674-678.

[8] Pieper, R.; Korpel, A.; Hereman, W. Extension of the acousto-optic Bragg regime through Hamming apodization of the sound field. *J. Opt. Soc. Am. A,* 3, 1608–1619, 1986.

[9] YUSHKOV, Konstantin B., CHIZHIKOV, Alexander I., et MOLCHANOV, Vladimir Ya. Acousto-optic transfer function control by a phased-array piezoelectric transducer. *Photonics*, vol. 10, no. 10, p. 1167, 2023.

[10] DUPONT, Samuel, KASTELIK, Jean-Claude, et VANHAMEL, Jurgen. Design and testing of a multi-electrode apodized acousto-optic filter for arbitrary polarized light. *Applied optics*, 2024, vol. 63, no 10, p. 2487-2493.

[11] KASTELIK, J.-C., DUPONT, Samuel, YUSHKOV, Konstantin B., *et al.* Double acousto-optic deflector system for increased scanning range of laser beams. *Ultrasonics*, 2017, vol. 80, p. 62-65.